

DIAMOND DOUBLE-CRYSTAL SYSTEM FOR A FORWARD BRAGG DIFFRACTION X-RAY MONOCHROMATOR OF THE SELF-SEEDED PAL XFEL

Yu. Shvyd'ko*, S. Kearney, K.-J. Kim, T. Kolodziej, D. Shu
 Argonne National Laboratory, Lemont, IL 60439, USA

V. D. Blank, S. Terentyev

Technological Institute for Superhard and Novel Carbon Materials, Troitsk, Russian Federation

H.-S. Kang, C.-K. Min, B. Oh

Pohang Accelerator Laboratory, Gyeongbuk, Republic of Korea

P. Vodnala, Northern Illinois University, DeKalb, IL 60115, USA

J. Anton, University of Illinois at Chicago, Chicago, IL 60607, USA

Abstract

PAL XFEL (Republic of Korea) is being planned to be operated in the self-seeded mode in a 3-keV to 10-keV photon spectral range. Monochromatization of x-rays in the self-seeding system will be achieved by forward Bragg diffraction (FBD) from two diamond single crystals in the [100] and [110] orientations (one at a time). We present results on the optical and engineering designs, on the manufacturing, and on the x-ray diffraction topography characterization of the diamond double-crystal systems for the FBD monochromator.

PHYSICAL REQUIREMENTS AND OPTICAL DESIGN

Seeded x-ray free-electron lasers (XFELs) [1, 2] generate fully coherent x-rays with a well-defined spectrum and high spectral flux. A hard x-ray self-seeding scheme uses x-rays from the first half of the FEL system (electron beam in a magnetic undulator system) to generate radiation by the self-amplified spontaneous emission process and seed the electron bunch in the second half of the FEL system via an x-ray monochromator [3, 4]. PAL XFEL [5] plans the hard x-ray self-seeding system operating in the spectral range from 3 keV to 10 keV, to be installed and commissioned in 2018. The concept of the system is based on the LCLS design [1], which utilizes the one-crystal forward Bragg diffraction (FBD) x-ray monochromator proposed at DESY [4].

X-rays in Bragg diffraction from a crystal, see Fig. 1, are emitted with a time delayed t upon excitation with an x-ray pulse and subsequent multiple scattering in the crystal either at a Bragg angle θ to the reflecting atomic planes (indicated in blue) or in the forward direction (in red). The FBD time response of an x-ray-transparent crystal, such as diamond, can be presented by the analytical expression [6, 7]

$$|G_{00}(t)|^2 \propto \left[\frac{1}{2\mathcal{T}_0} \frac{J_1 \left[\sqrt{\frac{t}{\mathcal{T}_0} \left(1 + \frac{t}{\mathcal{T}_d} \right)} \right]}{\sqrt{\frac{t}{\mathcal{T}_0} \left(1 + \frac{t}{\mathcal{T}_d} \right)}} \right]^2 \quad (1)$$

with the characteristic time parameters

$$\mathcal{T}_0 = \frac{2[\bar{\Lambda}_H^{(s)}]^2 \sin(\theta + \eta)}{cd}, \quad \mathcal{T}_d = \frac{2d \sin^2 \theta}{c|\sin(\theta - \eta)|}. \quad (2)$$

where \mathcal{T}_0 is the FBD time constant, see Fig. 1(c), $\bar{\Lambda}_H^{(s)}$ is the extinction length (a Bragg reflection invariant), $\mathbf{H} = (hkl)$ is the Bragg diffraction vector, d is the crystal thickness, η is the asymmetry angle between the crystal surface and the reflecting atomic planes, c is the speed of light, and J_1 is the Bessel function of the first kind. The FBD time response is shown by the red line in Fig. 1(c) for a particular case. The FBD photons are concentrated within a spectral bandwidth,

$$\Delta E_0 = \frac{\hbar}{\pi\mathcal{T}_0}, \quad (3)$$

see Fig. 1(b), which is typically larger than $\Delta E_H = \Delta E_0 (2\pi\bar{\Lambda}_H^{(s)}/d)$, the spectral width of BD, see Fig. 1(a).

The first trailing maximum of the FBD time response appears at time delay $t_s = 26\mathcal{T}_0$, see Fig. 1(c), and its duration is $\Delta t_s = 16\mathcal{T}_0$ (assuming $t \ll \mathcal{T}_d$). The intensity, delay, duration, and monochromaticity of the x-ray photons are defined by the single parameter \mathcal{T}_0 . For efficient seeding, we require that the peak of the electron bunch is delayed by t_s , to overlap with the first trailing maximum. The optimal delay is $t_s = 20 - 25$ fs. As a result, the FBD monochromator crystal parameters d , $\bar{\Lambda}_H^{(s)}$, θ , and η should be chosen such that $\mathcal{T}_0 \approx 0.75 - 1$ fs.

An x-ray pulse emanating from the crystal in FBD is not only delayed, it experiences also a lateral shift [6, 7]

$$x = tc \cot \theta, \quad (4)$$

proportional to the time delay t schematically shown in the left graph of Fig. 1. To ensure efficient seeding, the lateral shift x_s at the time delay t_s should be much smaller than the electron beam size, which is $\approx 25 \mu\text{m}$ (rms) for PAL XFEL.

A practically important question for the fabrication of the FBD monochromator crystals is an admissible angular spread $\Delta\theta_A$ of the crystal lattice deformation due to crystal defects or mounting strain. From Bragg's law $E = E_H \sin \theta$ ($E_H = hc/2d$ is a backreflection photon energy) the variation δE of the peak reflectivity in BD and of the FBD spectral function with angle is $\delta E = E_H \delta\theta \cos \theta$. If we require that

* shvydko@aps.anl.gov

Content from this work may be used under the terms of the CC BY 3.0 licence (© 2018). Any distribution of this work must maintain attribution to the author(s), title of the work, publisher, and DOI.

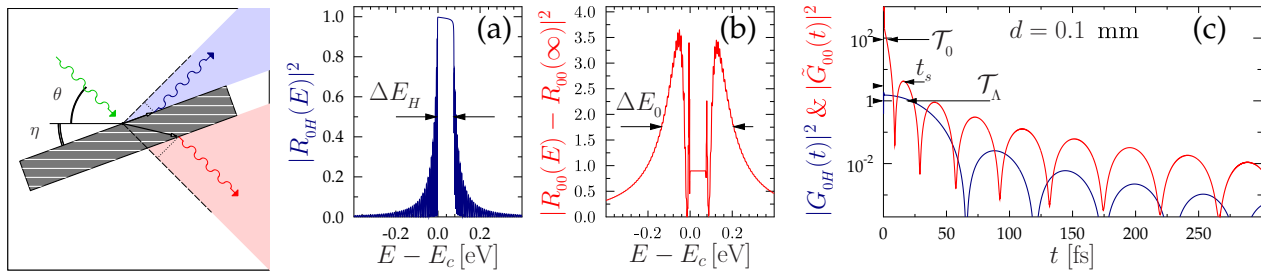


Figure 1: Schematic of Bragg diffraction (BD) and forward Bragg diffraction (FBD) of x-rays from a crystal (left). Examples of energy dependences of x-ray reflectivity $|R_{0H}(E)|^2$ in BD (a) and in FBD $|R_{00}(E) - R_{00}(\infty)|^2$ (b) from a diamond crystal in the (400) Bragg reflection, $E_c = 8.33$ keV, $\theta = 56.6^\circ$, $\eta = 0^\circ$, $d = 0.1$ mm. (c) Intensities of the corresponding time dependencies of crystal response to an excitation with an ultra-short x-ray pulse in BD $|G_{0H}(t)|^2$ (blue) and in FBD $|G_{00}(t)|^2$ (red).

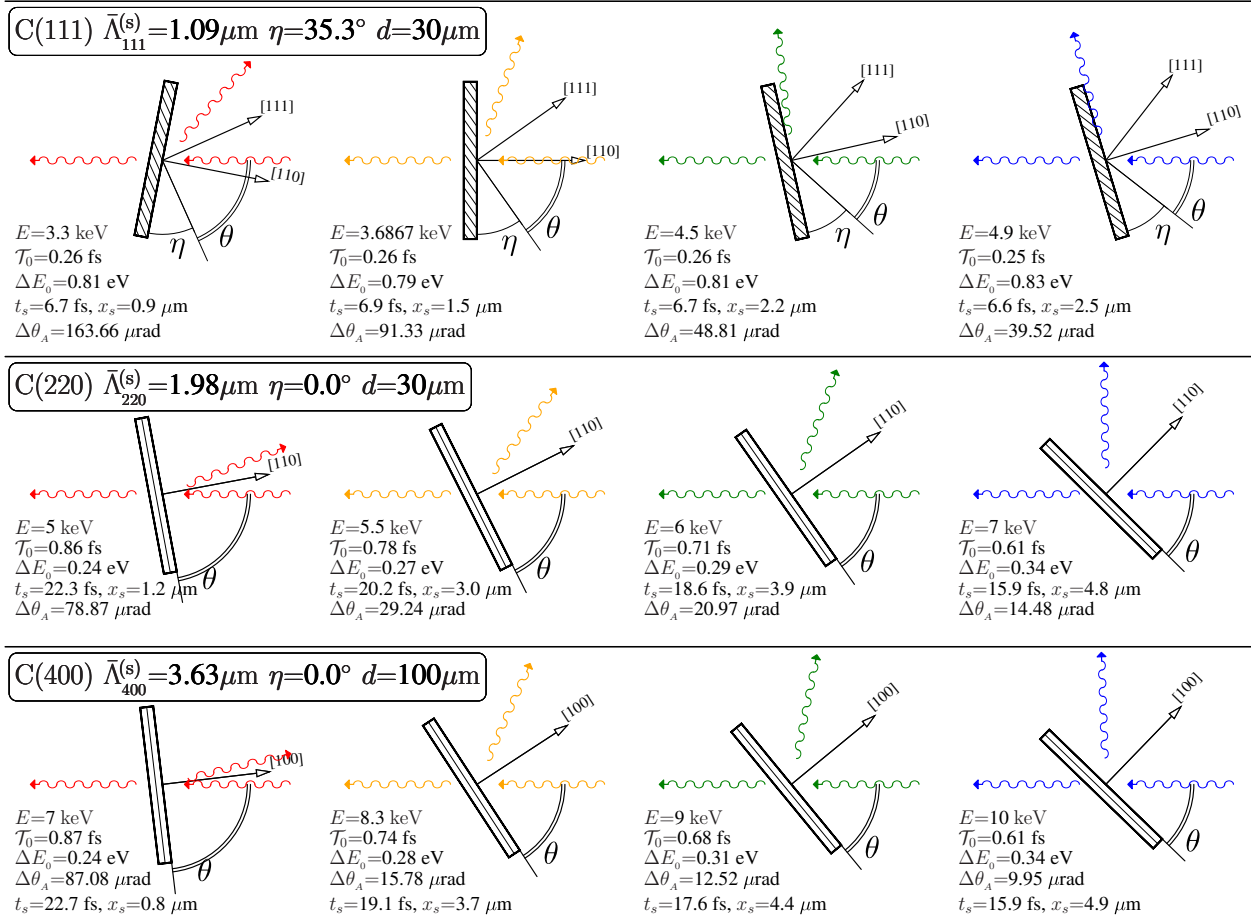


Figure 2: Bragg diffraction and forward Bragg diffraction scattering configurations shown together with diamond crystal and x-ray seed parameters in a $E = 3.3$ keV to $E = 10$ keV photon spectral range.

such variation should not exceed 5% of the FBD spectral bandwidth ΔE_0 , we obtain

$$\Delta\theta_A = 0.32 \frac{\Delta E_0}{E_H \cos \theta} \quad (5)$$

The spectral range of x-ray monochromatization from 6.9516 keV to 10 keV can be covered using the (400) Bragg diffraction from a 100 μm -thick diamond crystal in the [100] orientation. Figure 2(bottom) shows scattering geometries

for different photon energies E , and calculated values of the FBD characteristic time \mathcal{T}_0 , time delay of the first trailing maximum t_s , time-averaged spectral bandwidth ΔE_0 of the seed, lateral shift x_s at $t = t_s$, and the admissible angular broadening $\Delta\theta_A$. For all photon energies, the \mathcal{T}_0 , t_s , x_s , and $\Delta\theta_A$ values are in the desired range. Seeding at photon energies higher than 10 keV may also work, however, with lower efficiency because of too large x_s and too small $\Delta\theta_A$.

The spectral range from 4.916 keV to 7 keV can be covered using the (220) Bragg diffraction, see Fig. 2(center) from a diamond crystal in the [110] orientation. However, because of a much smaller $\bar{\Lambda}_{220}^{(s)} = 1.98 \mu\text{m}$, a much thinner crystal with $d = 30 \mu\text{m}$ has to be used to ensure the required \mathcal{T}_0 .

Using the (111) asymmetric Bragg reflection from the same crystal, see Fig. 2(top), the monochromatic seed in the spectral range from 3.3 keV to 5 keV can be generated. However, a twice smaller $\bar{\Lambda}_{111}^{(s)} = 1.09 \mu\text{m}$ for the (111) reflection, compared to that of the (220) reflection, results in \mathcal{T}_0 values out of the optimal range. Seeding may still take place, however, the electron bunch at the same delay will overlap with the radiation field having a more complex time structure (will overlap with the second and third trailing maxima) and therefore a more complex spectrum.

The above analysis suggests using two crystals (one at a time) a $100 \mu\text{m}$ -thick in the [100] orientation, for monochromatization in the 7 to 10 keV range with the (400) reflection, and a $30 \mu\text{m}$ -thick in the [110] orientation, for monochromatization in the 5 to 3.3 keV range with the symmetric (220) and the asymmetric (111) reflections.

Because manufacturing a $30 \mu\text{m}$ -thick crystal and mounting it strain-free is a challenge, a second back-up double-crystal diamond system was planned with a $90 \mu\text{m}$ -thick crystal in the [110] orientation.

ENGINEERING DESIGN AND MANUFACTURING

The mechanical design of the double-crystal system has to ensure (i) mechanically stable strain-free mount of the thin diamond crystals, (ii) a good heat transport and heat sink of the absorbed x-ray power by the crystals, and (iii) radiation-safe XFEL operations. The latter means that no metal parts are allowed within about 5 mm of the diamond crystals. A toothbrush-type mechanical design of the one-crystal FBD monochromator system for the LCLS self-seeding monochromator [8] was used as a prototype for the present design. Although it has proved to be viable, there were a few issues with the LCLS design. The diamond crystal was mounted in a graphite holder to comply with radiation safety requirements. However, the heat transport in graphite is very poor. Besides, the graphite holder does not allow easy and reliable control of the crystal mounting strain. The present design is aimed at keeping close to the LCLS standard and improving the mentioned drawbacks.

The new design features include:

1. The two diamond single-crystal plates in two different crystallographic orientations are mounted on a common base.
2. The base is manufactured from polycrystalline diamond grown with the chemical vapor deposition (CVD) method, to ensure a good heat transport through GaIn eutectic.
3. Thin graphite springs are used to press gently the diamond crystals to the base. Thin graphite springs are softer than the thin perforated diamond springs applied

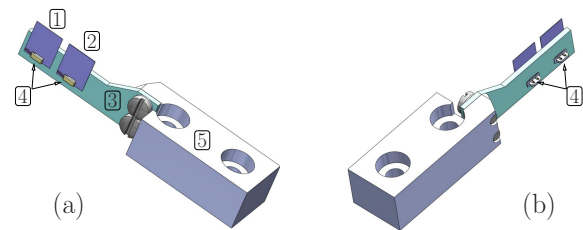


Figure 3: Drawings of the diamond two-crystal system for the FBD monochromator. Front (a) and back (b) views of the system are shown. Two diamond monochromator crystals C*[100] - 1 - and C*[110] - 2 - are mounted on the CVD-diamond base - 3 - using diamond posts and graphite springs - 4. The CVD base is attached to the graphite holder - 5.

in [9] and are still radiation safe. The pressure on the diamond crystals can be controlled by changing the springs' thickness. The diamond posts holding the springs are now firmly attached to the CVD bases as detailed in [10]. As a result, the crystals will still stay in place even if the graphite springs fall out.

4. The CVD diamond base is attached to a graphite holder, with mounting holes and dimensions equivalent to those of the LCLS design.
5. The lower narrow facet of the base can be attached to a heat sink.

Drawings of the diamond two-crystal system for the FBD monochromator are presented in Fig. 3. The system has a total length of 35.5 mm. The monochromator diamond crystals (1) and (2) are $\approx 4 \text{ mm(H)} \times 5 \text{ mm(V)}$ each. They are laser cut from the highest quality type-IIa diamond crystal grown by the high-pressure high-temperature technique (see [11] for references) and polished to a 5 nm (rms) surface micro-roughness. The $19.6 \text{ mm} \times 6 \text{ mm}$ and 0.75-mm-thick supporting CVD base (3) is machined by laser cutting. The monochromator crystals are attached to the CVD base by an assembly (4) with diamond crystal posts, graphite flat springs, and graphite wedges, as detailed in [10]. The graphite springs thickness is in the $\approx 50 - 100 \mu\text{m}$ range.

Two diamond double-crystal systems manufactured according to the design specifications and Fig. 3 drawings are shown on in Fig. 4. The systems and all their components were manufactured at Technological Institute for Superhard and Novel Carbon Materials (TISNCM, Russia).

X-RAY DOUBLE-CRYSTAL TOPOGRAPHY CHARACTERIZATION

The crystal quality of the monochromator diamond crystals has been characterized by sequential x-ray Bragg diffraction topography. The technique measures Bragg reflection images of a crystal with a pixel x-ray detector sequentially at different incidence angles to the reflecting atomic planes of well collimated x-rays. The angular dependences of Bragg reflectivity (rocking curves) measured with each detector pixel are used to calculate Bragg reflection maps of the angular widths of the rocking curves, and the maps of the center of mass (COM) of the rocking curves are shown as color

Content from this work may be used under the terms of the CC BY 3.0 licence (© 2018). Any distribution of this work must maintain attribution to the author(s), title of the work, publisher, and DOI.

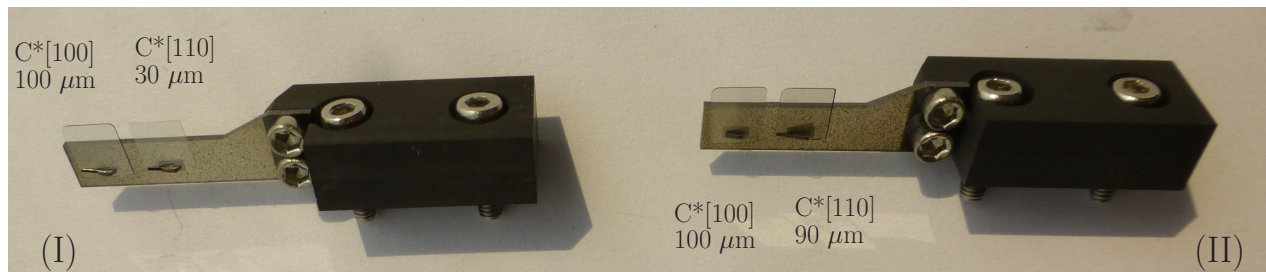


Figure 4: Photograph of the diamond double-crystal systems I and II manufactured according to the Fig. 3 drawings. The monochromator diamond single-crystal plates C^* are attached to the CVD-diamond crystal bases. Both $C^*[100]$ crystals (left in each system) are $100\ \mu\text{m}$ thick. The $C^*[110]$ crystals (right in each system) are $30\ \mu\text{m}$ and $90\ \mu\text{m}$ thick, respectively. All crystals are $\approx 4 \times 5\ \text{mm}^2$ in size.

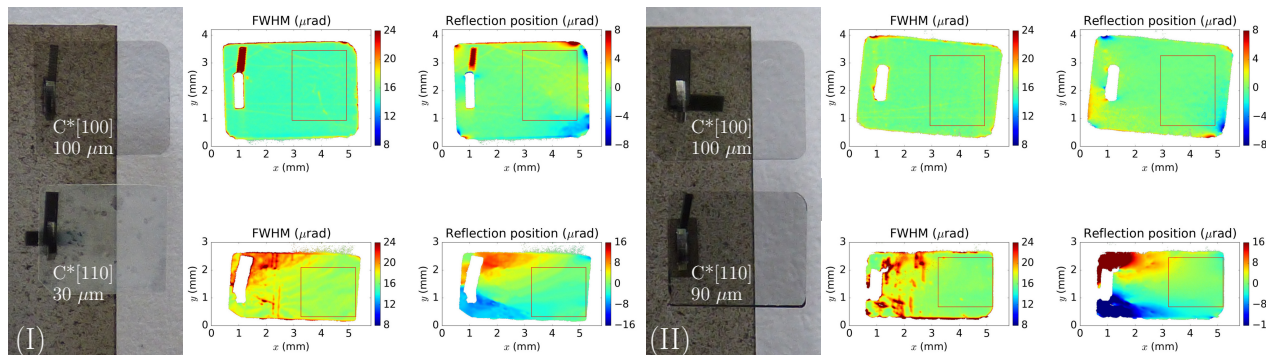


Figure 5: Photographs and Bragg reflection rocking curve color maps of the diamond FBD monochromator crystals. Shown are color maps of the reflection angular widths (FWHM) and of the reflection angular positions. The graphs in the upper row correspond to the crystals in the $[100]$ orientation, while the bottom row graphs to the crystals in the $[110]$ orientation. The graphs on the left half belong to diamond double-crystal system I, while those of system II are on the right half. Red rectangles on the maps indicate the working regions, featuring almost theoretical Bragg reflection widths and less than $1.5\ \mu\text{rad}$ (rms) reflection position angular variations.

maps in Fig. 5. Microscopic defect structure can be derived from the Bragg reflection images and Bragg reflection width maps. Mesoscopic and macroscopic defects or crystal strain can be best evaluated from the COM maps.

We have used a sequential x-ray diffraction topography setup at 1-BM X-ray Optics Testing Beamline at the Advanced Photon Source (APS, USA) [12]. The setup employs a nearly-nondispersive double-crystal $\text{Si}(531)\text{-C}^*(400)$ Bragg diffraction arrangement to characterize diamond crystals in the $[100]$ orientation, and a $\text{Si}(111)\text{-C}^*(220)$ arrangement to characterize diamond crystals in the $[110]$ orientation. In each arrangement, the first crystal is an asymmetrically cut high-quality silicon conditioning crystal, and the second one is a diamond crystal under investigation. The setup enables rocking curve mapping with a submicroradian angular and $13\ \mu\text{m}$ spatial resolution. The spatial resolution is limited by the detector pixel size.

Figure 5 shows photographs and Bragg reflection rocking curve color maps of the diamond FBD monochromator crystals. Scales on the x - and y -axis in Fig. 5 correspond to the detector coordinates. The crystals at the Bragg angle θ to the detector plane therefore appear to be contracted in the y direction by a factor of $\sin \theta = 0.85$ for the (400) Bragg reflection from the diamond crystal ($8.2\ \text{keV}$ x-rays) and by

a factor of $\sin \theta = 0.6$ for the (220) Bragg reflection. The maps were calculated using a dedicated code [13].

The double-crystal x-ray topography reveals that the crystals in working areas of $2\ \text{mm}(V) \times 2\ \text{mm}(H)$ indicated in Fig. 5 by red rectangles are almost flawless, with the reflection width close to the theoretical values and the mounting strain $\lesssim 1.5\ \mu\text{rad}$ (rms), well below the admissible $\Delta\theta_A$ values given in Fig. 2. It should be noted however, that as manufactured $30\ \mu\text{m}$ thin crystals in the $[110]$ orientation featured much larger strain. The strain has been reduced substantially by annealing the crystal for 3 hours in a muffle furnace in air at a temperature of $920\ \text{K}$, as described in [14]. Although the crystal surface became more rough and the crystal optically less transparent after annealing, no problems are expected regarding its performance as the x-ray FBD monochromator.

CONCLUSIONS

A double-crystal system composed of a $100\ \mu\text{m}$ -thick diamond crystal in the $[100]$ orientation and a $30\ \mu\text{m}$ -thick diamond crystal in the $[110]$ orientation mounted on a common CVD-diamond base was designed and manufactured for use as a forward Bragg diffraction monochromator in the $3.3\ \text{keV}$ to $10\ \text{keV}$ spectral range of the self-seeded PAL XFEL. A second back-up system was manufactured with a

thicker (90 μm) diamond crystal in [110] orientation. The crystals are mounted in a mechanically stable fashion using diamond and graphite components, ensuring proper x-ray monochromatization, heat transport, mechanical stability, and radiation-safe XFEL operations. The double-crystal x-ray topography revealed that the crystals in a working area of about $2 \times 2 \text{ mm}^2$ are almost flawless and the mounting strain is $\leq 1.5 \mu\text{rad}$ (rms), i.e., well below the admissible values. We expect that the monochromator crystals will perform close to the design specifications.

ACKNOWLEDGMENTS

Dr. Stanislav Stoupin is acknowledged for technical support at the Advanced Photon Source (APS) 1-BM beamline and making available the software for the evaluation of the x-ray topography data. Dr. Albert Macrander and Dr. Lahsen Assoufid are acknowledged for supporting this research at the 1-BM beamline. Work at Argonne National Laboratory was supported by the U.S. Department of Energy, Office of Science, Office of Basic Energy Sciences, under contract DE-AC02-06CH11357. Work at TISCNM was supported by the Ministry of Education and Science of Russian Federation: scientific project RFMEF1586114X0001 Grant No. 14.586.21.0001. Work at PAL XFEL was supported by the Ministry of Science and ICT, Republic of Korea.

REFERENCES

- [1] J. Amann, W. Berg, V. Blank, F.-J. Decker, Y. Ding, P. Emma, Y. Feng, J. Frisch, D. Fritz, J. Hastings, Z. Huang, J. Krzywinski, R. Lindberg, H. Loos, A. Lutman, H.-D. Nuhn, D. Ratner, J. Rzepiela, D. Shu, Yu. V. Shvyd'ko, S. Spampinati, S. Stoupin, S. Terentiev, E. Trakhtenberg, D. Walz, J. Welch, J. Wu, A. Zholents, and D. Zhu, "Demonstration of self-seeding in a hard-x-ray free-electron laser", *Nature Photonics*, 6, 2012.
- [2] E. Allaria, R. Appio, L. Badano, W.A. Barletta, S. Bassanese, S.G. Biedron, A. Borgia, E. Busetto, D. Castronovo, P. Cinquegrana, S. Cleva, D. Cocco, M. Cornacchia, P. Craievich, I. Cudin, G. D'Auria, and et al. "Highly coherent and stable pulses from the fermi seeded free-electron laser in the extreme ultraviolet", *Nature Photonics*, 6:699–704, 2012.
- [3] E. L. Saldin, E. A. Schneidmiller, Yu. V. Shvyd'ko, and M. V. Yurkov. "X-ray FEL with a meV bandwidth" *Nucl. Instrum. Methods Phys. Res. A*, 475:357–362, 2001.
- [4] G. Geloni, V. Kocharyan, and E. L. Saldin. "A novel self-seeding scheme for hard x-ray FELs", *Journal of Modern Optics*, 58:1391–1403, 2011.
- [5] I.S. Ko, H.-S. Kang, H. Heo, C. Kim, G. Kim, C.-K. Min, H. Yang, S.Y. Baek, H.-J. Choi, G. Mun, B.R. Park, Y.J. Suh, D.C. Shin, J. Hu, J. Hong, S. Jung, S.-H. Kim, K. Kim, D. Na, S.S. Park, Y.J. Park, Y.G. Jung, S.H. Jeong, H.G. Lee, S. Lee, S. Lee, B. Oh, H.S. Suh, J.-H. Han, M.H. Kim, N.-S. Jung, Y.-C. Kim, M.-S. Lee, B.-H. Lee, C.-W. Sung, I.-S. Mok, J.-M. Yang, Y.W. Parc, W.-W. Lee, C.-S. Lee, H. Shin, J.H. Kim, Y. Kim, J.H. Lee, S.-Y. Park, J. Kim, J. Park, I. Eom, S. Rah, S. Kim, K.H. Nam, J. Park, J. Park, S. Kim, S. Kwon, R. An, S.H. Park, K.S. Kim, H. Hyun, S.N. Kim, S. Kim, C.-J. Yu, B.-S. Kim, T.-H. Kang, K.-W. Kim, S.-H. Kim, H.-S. Lee, H.-S. Lee, K.-H. Park, T.-Y. Koo, D.-E. Kim, K.B. Lee, "Construction and commissioning of PAL-XFEL facility", *Applied Sciences*, 7(5), 2017.
- [6] R. R. Lindberg and Yu. V. Shvyd'ko "Time dependence of Bragg forward scattering and self-seeding of hard x-ray free-electron lasers", *Phys. Rev. ST Accel. Beams*, 15:050706, May 2012.
- [7] Yu. V. Shvyd'ko and R. Lindberg, "Spatiotemporal response of crystals in x-ray Bragg diffraction" *Phys. Rev. ST Accel. Beams*, 15:100702, Oct 2012.
- [8] S. Stoupin, V. D. Blank, S. A. Terentyev, S.N. Polyakov, V.N. Denisov, M. S. Kuznetsov, Yu. V. Shvyd'ko, D. Shu, P. Emma, J. Maj, and J. Katsoudas, "Diamond crystal optics for self-seeding of hard x-rays in x-ray free-electron lasers", *Diamond and Related Materials*, 33:1–4, 2013.
- [9] S. Stoupin, S. A. Terentyev, V. D. Blank, Yu. V. Shvyd'ko, K. Goetze, L. Assoufid, S. N. Polyakov, M. S. Kuznetsov, N. V. Kornilov, J. Katsoudas, R. Alonso-Mori, M. Chollet, Y. Feng, J. M. Glowina, H. Lemke, A. Robert, M. Sikorski, S. Song, and D. Zhu, "All-diamond optical assemblies for a beam-multiplexing X-ray monochromator at the Linac Coherent Light Source", *Journal of Applied Crystallography*, 47(4):1329–1336, Aug 2014.
- [10] S. Terentyev, V. Blank, T. Kolodziej, and Yu. V. Shvyd'ko, "Curved diamond-crystal spectrographs for x-ray free-electron laser noninvasive diagnostics", *Rev. Sci. Instrum.*, 87:125117, 2016.
- [11] Yu. V. Shvyd'ko, V. Blank, and S. Terentyev, "Diamond x-ray optics: Transparent, resilient, high-resolution, and wavefront preserving", *MRS Bulletin*, 62(6):437–444, 2017.
- [12] S. Stoupin, Yu. V. Shvyd'ko, E. Trakhtenberg, Z. Liu, K. Lang, X. Huang, M. Wiczorek, E. Kasman, J. Hammonds, A. Macrander, and L. Assoufid, "Sequential x-ray diffraction topography at 1-BM x-ray optics testing beamline at the Advanced Photon Source", *AIP Conf. Proc.*, 1471:050020, 2016.
- [13] S. Stoupin, "Python-DTXRD", <https://www1.aps.anl.gov/science/scientific-software/dtxrd> 2015.
- [14] T. Kolodziej, P. Vodnala, S. Terentyev, V. Blank, and Yu. V. Shvyd'ko, "Diamond drumhead crystals for X-ray optics applications", *Journal of Applied Crystallography*, 49(4):1240–1244, Aug 2016.